Zinc transporter 10 (ZnT10)-dependent extrusion of cellular Mn^{2+} is driven by an active Ca^{2+}-coupled exchange

Received for publication, November 22, 2018, and in revised form, January 30, 2019 Published, Papers in Press, February 12, 2019, DOI 10.1074/jbc.RA118.006816

Moshe Levy[‡1], Nadav Elkoshi[‡1], Shiran Barber-Zucker[§], Eitan Hoch[¶], Raz Zarivach[§], Michal Hershfinkel[‡], and Israel Sekler[‡2]

From the [‡]Department of Physiology and Cell Biology, Faculty of Health Sciences, Ben-Gurion University of the Negev, Beer Sheva 8410501 Israel, [¶]Program in Medical and Population Genetics and Metabolism Program, Broad Institute of MIT and Harvard, Cambridge, Massachusetts 02142, and [§]Department of Life Sciences and The National Institute for Biotechnology in the Negev and Ilse Katz Institute for Nanoscale Science and Technology, Ben-Gurion University of the Negev, Beer Sheva 8410501 Israel

Edited by Roger J. Colbran

Manganese (Mn^{2+}) is extruded from the cell by the zinc transporter 10 (ZnT10). Loss of ZnT10 expression caused by autosomal mutations in the *ZnT10* gene leads to hypermanganesemia in multiple organs. Here, combining fluorescent monitoring of cation influx in HEK293-T cells expressing human ZnT10 with molecular modeling of ZnT10 cation selectivity, we show that ZnT10 is exploiting the transmembrane Ca^{2+} inward gradient for active cellular exchange of Mn^{2+}. In analyzing ZnT10 activity we used the ability of Fura-2 to spectrally distinguish between Mn^{2+} and Ca^{2+} fluxes. We found that (*a*) application of Mn^{2+}-containing Ca^{2+}-free solution to ZnT10-expressing cells triggers an influx of Mn^{2+}, (*b*) reintroduction of Ca^{2+} leads to cellular Mn^{2+} extrusion against an inward Mn^{2+} gradient, and (*c*) the cellular transport of Mn^{2+} by ZnT10 is coupled to a reciprocal movement of Ca^{2+}. Remarkably, replacing a single asparagine residue in ZnT10 (Asp-43) with threonine (ZnT10 N43T) converted the Mn^{2+}/Ca^{2+} exchange to an uncoupled channel mode, permeable to both Ca^{2+} and Mn^{2+}. The findings in our study identify the first ion transporter that uses the Ca^{2+} gradient for active counter-ion exchange. They highlight a remarkable versatility in metal selectivity and mode of transport controlled by the tetrahedral metal transport site of ZnT proteins.

The mammalian SLC30 (solute-like carrier 30)[3] family of Zn^{2+} transporters (ZnT) includes 10 membrane-embedded proteins (1) and is part of the broader cation diffusion facilitator (CDF) family that spans across bacteria, fungi, and plants (2). ZnTs are associated with numerous Zn^{2+}-related pathophysiologies, for instance Alzheimer's (5, 6), and type II diabetes (7, 8). Most mammalian ZnT members mediate cellular and vesicular Zn^{2+} transport by exchanging it with H^+ (3, 4). Despite their modest general sequence homology, ZnT members share a conserved tetrahedral metal transport site with plant, fungal, and bacterial transporters (4, 9, 10).

In contrast to other ZnT members that transport Zn^{2+}, ZnT10 emerges as a Mn^{2+} transporter (11–13). This novel function was first discovered by analysis of homozygous mutations in human ZnT10 gene. Patients carrying these mutations manifested severe hypermanganesemia associated with onset of parkinsonism, polycythemia, and chronic liver disease (14, 15). These studies were followed by functional analysis in neurons showing that ZnT10 is linked to Mn^{2+} efflux, which is critically determined by an asparagine (Asn) residue replacing a conserved histidine (His) at the tetrahedral metal transport site of ZnT10 (14, 15). How ZnT10 is able to mediate Mn^{2+} extrusion is unknown however. Manganese gradient across the cell membrane is very steep and can reach more than 3000-fold (16). Moreover, in contrast to Zn^{2+}, Mn^{2+} is redox active and may induce oxidative damage (17, 18). Hence, removal of Mn^{2+} requires a counter ion distributed in an electrochemical gradient that can power the cellular extrusion of Mn^{2+}. Although vesicular H^+ gradient may reach 100-fold (19), the magnitude of the H^+ gradient across the cell membrane is only ~5- to 10-fold (20), which would be insufficient to support cellular Mn^{2+} extrusion. In contrast, Ca^{2+} is distributed at 4–5 orders of magnitude inward facing electrochemical gradient across the cell membrane and thus could potentially provide the driving force for Mn^{2+} efflux (21).

Here we show that ZnT10-dependent Mn^{2+} efflux is coupled to Ca^{2+} exchange. Hence, ZnT10 is the first known ion transporter that utilizes the steep transmembrane Ca^{2+} gradient. Finally, we demonstrate that a single mutation in the ZnT10 metal transport site renders ZnT10 exchanger to a cationic-like channel.

Results

Functional analysis of Mn^{2+} and Zn^{2+} transport by ZnT10

The properties of ZnT10 metal selectivity are not fully resolved. Specifically it is not clear whether ZnT10 transports both Zn^{2+} and Mn^{2+} (22, 23) or only Mn^{2+} (24). To determine whether ZnT10 mediates Zn^{2+} transport we monitored cellu-

This work was supported by Israel Science Foundation Grants ISF 1429/17 ISF-China 1210/14 and DIP SE2372/1–1 (to I. S.) and ISF 891/14 (to M. H.) and by the Israel Ministry of Science, Technology and Space, Israel Science Foundation Grant 167/16) (to R. Z. and S. B. -Z.). This work is also supported by the European Molecular Biology Organization and CMST COST Action CM1306. The authors declare that they have no conflicts of interest with the contents of this article.

This article contains Figs S1–S3 and Tables S1–S5.

[1] These authors contributed equally to this work

[2] To whom correspondence should be addressed. Tel.: 972-8-6477328; E-mail: Sekler@bgu.ac.il.

[3] The abbreviations used are: SLC30, solute-like carrier 30; ZnT, Zn^{2+} transporters; NMDG, *N*-methyl-D-glucamine; CDF, cation diffusion facilitator; BLAST, Basic Local Alignment Search Tool; a.u., arbitrary unit; ANOVA, analysis of variance.

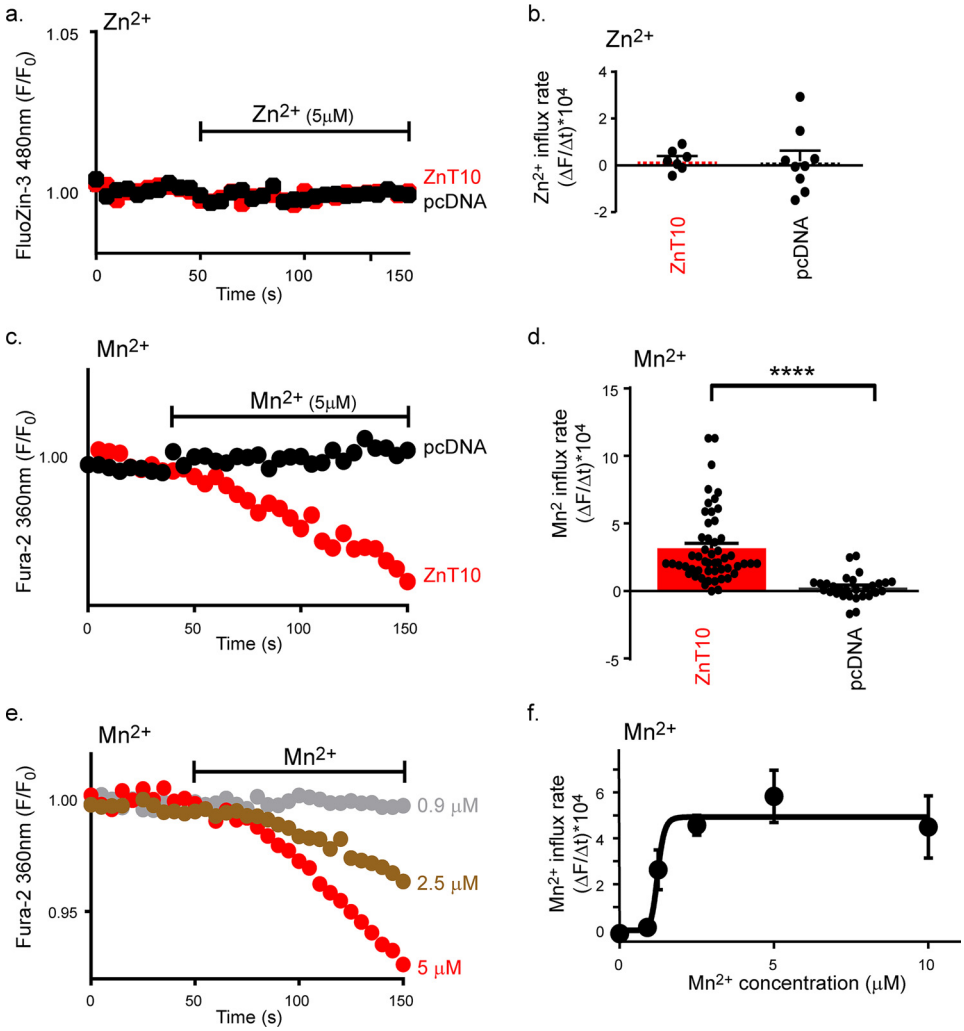

Figure 1. ZnT10 mediates Mn^{2+} but not Zn^{2+} transport. *a*, representative traces of Zn^{2+} influx in ZnT10 (*red*) *versus* pcDNA (*black*) transfected cells loaded with FluoZin-3 and monitored for cytoplasmic Zn^{2+} transport. Cells were initially superfused with Ringer's solution and then with Ringer's solution containing Zn^{2+} (50 μM) at the time intervals indicated by the *horizontal bar*. *b*, mean rates of cytoplasmic Zn^{2+} uptake for ZnT10 ($n = 7$) and pcDNA ($n = 9$) taken from *a* (unpaired *t*-test). *c*, representative traces of Mn^{2+} influx in ZnT10 (*red*) *versus* pcDNA (*black*) transfected cells loaded with Fura-2AM and monitored for cytoplasmic Mn^{2+} transport. Cells were initially superfused with Ringer's Ca^{2+}-free solution and then with Ringer's Ca^{2+}-free solution containing Mn^{2+} (5 μM) applied as indicated by the *horizontal bar*. *d*, mean rates of cytoplasmic Mn^{2+} uptake for ZnT10 ($n = 52$) and pcDNA ($n = 29$) taken from *c* (unpaired *t*-test; ****, $p < 0.0001$). *e*, representative traces of Mn^{2+} dose-response analysis of ZnT10 transfected cells. Mn^{2+} was added at the indicated concentrations and Mn^{2+} influx was monitored as described in *c*. *f*, mean rates of cellular Mn^{2+} uptake taken from *e* as a function of Mn^{2+} concentration (allosteric sigmoidal fit; $n = 4$; $K_{1/2} = 1.235 \pm 0.064$, μM; $V_{max} = 4.931 \pm 0.477$, a.u.).

lar Zn^{2+} influx in HEK293-T cells expressing human ZnT10 or transfected with vector alone (pcDNA). Cells were preloaded with the high-affinity fluorescent Zn^{2+} dye, FluoZin-3AM and were then superfused with a 50 μM Zn^{2+}-containing, Ca^{2+}-free, Ringer's solution. Despite the presence of high Zn^{2+} concentration in the solution, and in agreement with previous studies (11, 13, 25), no increase in cellular Zn^{2+} influx was observed in cells expressing ZnT10 (Fig. 1, *a* and *b*). Fura-2AM is a widely used Ca^{2+} reporter that was also previously used as a Mn^{2+}-sensitive dye when excited at 360 nm wavelength (26). When cells were perfused with Mn^{2+}-containing, Ca^{2+}-free, Ringer's solution, the Mn^{2+} influx rate in ZnT10-expressing cells was increased by more than 10-fold compared with control cells (Fig. 1, *c* and *d*). Using the same paradigm we then performed Mn^{2+} dose-response analysis (Fig. 1, *e* and *f*) and found that ZnT10 is capable of conducting high-affinity Mn^{2+} transport with a $K_{1/2} = 1.235 \pm 0.064$ μM.

ZnT10 does not utilize the H^+ or Na^+ transmembrane gradient for Mn^{2+} transport

All known ZnT family members use a H^+-driven gradient for metal exchange (4). We therefore asked if ZnT10 also utilizes transmembrane H^+ gradients for transport of Mn^{2+}. We used the same protocol for Mn^{2+} uptake as described in Fig. 1*c* while superfusing the cells with Ringer's solutions titrated at an extracellular pH range of 6–8 (Fig. 2*a*). At pH values of 7.4 and 8, Mn^{2+} influx was maximal, diminished at pH 7 and was totally blocked at the acidic pH 6 (Fig. 2, *a* and *b*). Such modulation of Mn^{2+} influx rate by pH can be either linked to regulation by pH or to direct H^+ coupled transport. To distinguish between these two mechanisms, we first asked if ZnT10 can utilize the H^+ gradient to support Mn^{2+} efflux. We loaded the cells with Mn^{2+} exploiting the Mn^{2+} influx mode of ZnT10 at pH 7.4, by superfusing ZnT10-expressing cells with Mn^{2+}-containing

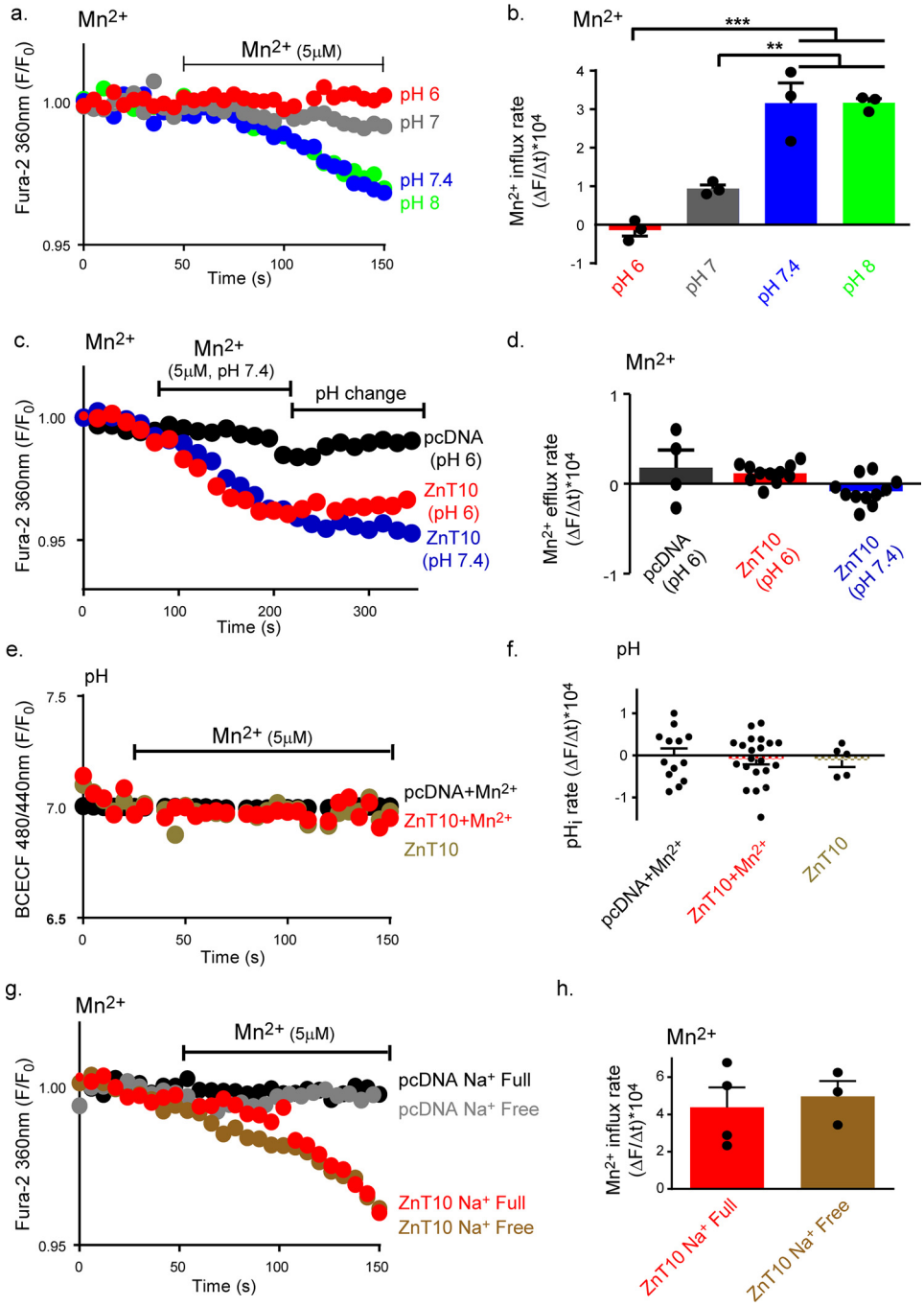

Figure 2. ZnT10 is regulated by pH but does not conduct H^+/Mn^{2+} or Na^+/Mn^{2+} exchange. *a*, representative traces of Mn^{2+} (5 μM) uptake in ZnT10 transfected cells. Cells were superfused with Ringer's solution at the indicated pH values. Mn^{2+} influx was monitored as described in Fig. 1*c*. *b*, mean rates of cellular Mn^{2+} uptake derived from *a* (one-way ANOVA test; $n = 3$; ***, $p < 0.001$; **, $p < 0.01$). *c*, Mn^{2+} efflux in cells expressing ZnT10 is unaffected by extracellular pH changes. Representative traces of Mn^{2+} (5 μM) transport in ZnT10 (*blue* and *red*) and pcDNA (*black*) transfected cells that were loaded with Fura-2AM and monitored at the indicated pH values. Cells were first superfused as in Fig. 1*c* with pH 7.4 Ringer's solution containing Mn^{2+} (5 μM) as indicated by the *left horizontal bar*, then as indicated by the *right horizontal bar* with Mn^{2+}-free Ringer at either pH 7.4 Ringer's solution (*blue*) or pH 6 (*red* and *black*) Ringer's solution. *d*, mean rates of cytoplasmic Mn^{2+} fluxes of cells superfused with a Ringer's solution at pH 7.4 ($n = 11$) or pH 6 (one-way ANOVA test, ZnT10 $n = 11$; pcDNA $n = 4$) taken from *c*. *e*, representative traces of cellular pH_i values in ZnT10 (*red* and *cream*) or pcDNA (*black*) transfected cells preloaded with BCECF-AM. Ringer's solution with (*red* and *black*) or without (*cream*) Mn^{2+} (5 μM) that was added as indicated by the *horizontal bar*. *f*, mean rates of cytoplasmic pH changes taken from *e* of Mn^{2+}-treated ZnT10 ($n = 21$), pcDNA ($n = 13$), and Mn^{2+} untreated ZnT10 ($n = 5$) transfected cells (one-way ANOVA test). *g*, effect of Na^+ on Mn^{2+} transport by ZnT10. Representative traces of Mn^{2+} (5 μM) influx in ZnT10 (*red* and *brown*) *versus* pcDNA (*black* and *gray*) transfected cells loaded with Fura-2AM and monitored for cytoplasmic Mn^{2+} transport as described in *c*. Cells were superfused with Na^+ full Ringer's solution containing Mn^{2+} (*red* and *black*) or Na^+-free NMDG buffer containing Mn^{2+} (*brown* and *gray*) as indicated in the graph. *h*, mean rates of cellular Mn^{2+} uptake of ZnT10 transfected cells in Na^+ full (*red*, $n = 4$) or Na^+-free (*brown*, $n = 3$) Ringer's solution. Data are derived from *g* and normalized to the background (unpaired *t*-test).

Ringer's solution. This was followed by superfusion with Mn^{2+}-free Ringer's, and comparison of rates of Mn^{2+} efflux at pH 7.4 *versus* pH 6 (Fig. 2, *c* and *d*). No change in Mn^{2+} efflux rate at any of these pH values was observed (Fig. 2, *c* and *d*). Another criterion for H^+-coupled exchange, previously shown for ZnT members and YiiP (4), is a metal-driven

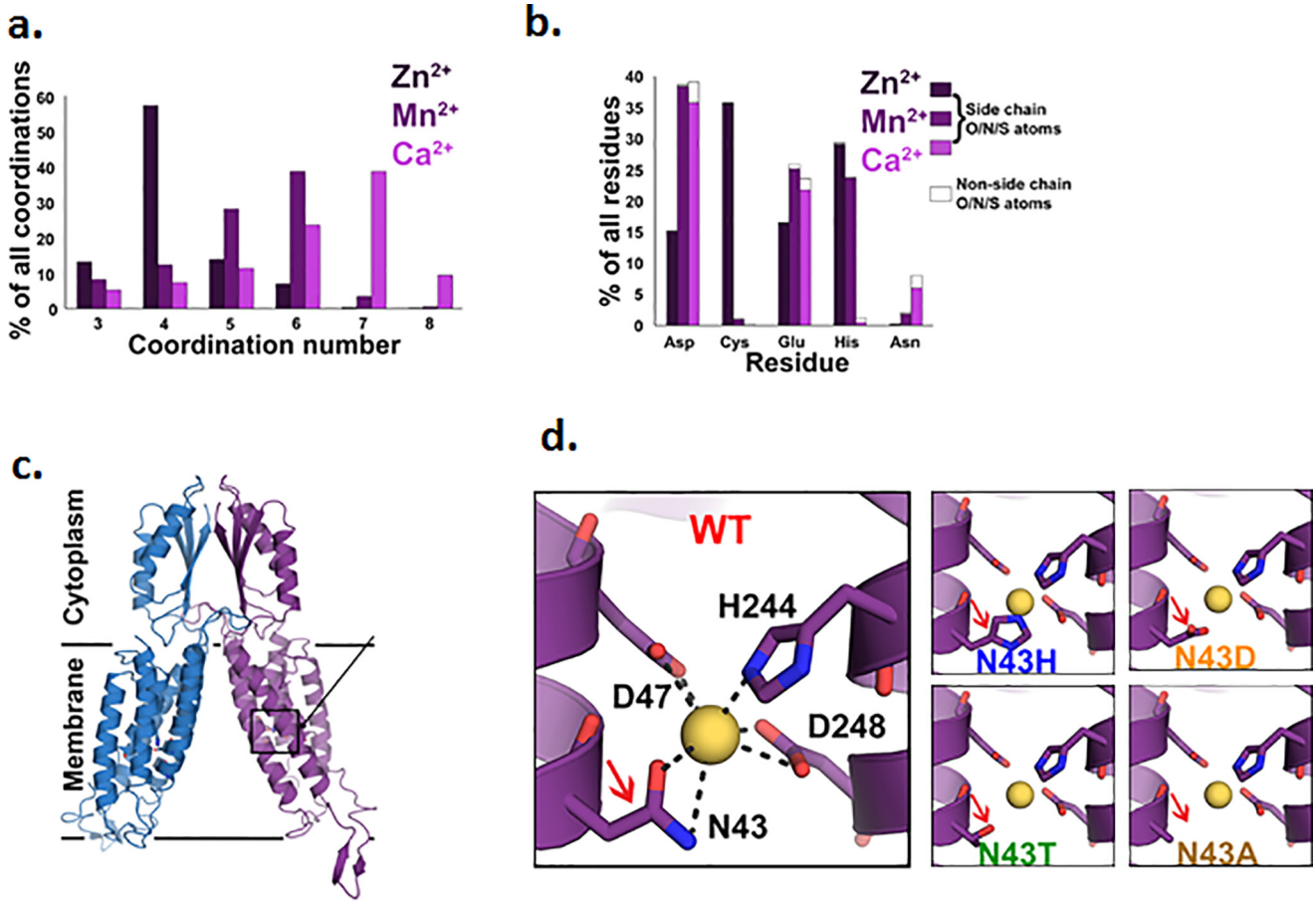

Figure 3. Data analysis poses Ca^{2+} as a possible candidate to support Mn^{2+} exchange by ZnT10. *a*, coordination number statistics of (left to right) Zn^{2+} (*dark purple*), Mn^{2+} (*purple*), and Ca^{2+} (*pink*) show strong preferences for 4-coordination of Zn^{2+} and higher coordination number preferences for both Mn^{2+} (5, 6) and Ca^{2+} (6, 7). *b*, selected amino acid tendencies of (left to right) Zn^{2+} (*dark purple*), Mn^{2+} (*purple*), and Ca^{2+} (*pink*). Filled parts refer to the percentage of the side-chain's polar atoms that are bound to the metal. *c*, structural model of ZnT10 was calculated based on the X-ray structure of the CDF protein YiiP (PDB code: 3H90) (48). Each monomer is represented in a different color, A-site residues are presented in *sticks*. Unstructured domains that are not presented in the model are residues 1–7, the His-rich loop (residues145–226), and the C-terminal (residues 386–485). *d*, magnification of the tetrahedral binding site: ZnT10 WT site occupied with Mn^{2+} ion in *yellow* (radius of 0.9 Å), ZnT10 Asn-43 substitution to His (ZnT10 N43H) creates tighter site and different coordination ability of the metal, ZnT10 Asn-43 substitution to Asp (ZnT10 N43D) maintains the cavity size but adds an extra charge, ZnT10 Asn-43 substitution to Thr (ZnT10 N43T) creates similar-sized polar cavity and ZnT10 Asn-43 substitution to Ala (ZnT10 N43A) creates a bigger cavity but neutralizes the site.

counter H^+ transport manifested by pH_i change. We therefore compared cytosolic pH changes in ZnT10- or vector-expressing cells loaded with the intracellular fluorescent pH indicator BCECF. No Mn^{2+}-dependent pH_i changes in either ZnT10- or vector-expressing cells were observed (Fig. 2, *e* and *f*). Altogether, this set of experiments indicates that although ZnT10 can be regulated by extracellular pH it does not utilize the H^+ gradient for mediating a counter H^+/Mn^{2+} transport.

Previous studies reported a Na^+-dependent Zn^{2+} efflux (27). Further, transmembrane Na^+ gradient is used by numerous Na^+ coupled exchangers. We therefore asked if ZnT10 conducts Na^+/Mn^{2+} exchange. We used the same paradigm for Mn^{2+} uptake as described in Fig. 1*c*, perfusing cells in the presence or absence of extracellular Na^+ that was isoosmotically replaced by NMDG. No difference in Mn^{2+} influx rate was monitored in cells superfused with Na^+-containing or Na^+-free Ringer's, indicating that ZnT10 does not conduct Na^+-dependent Mn^{2+} transport (Fig. 2, *g* and *h*).

ZnT10 is the first known transporter that utilizes the Ca^{2+} gradient

Because H^+ or Na^+ failed to support ZnT10-dependent Mn^{2+} transport, we asked if the transport site can bind Ca^{2+}. Applying a structural/modeling-based comprehensive analysis, we scanned the RCSB Protein Data Bank and extracted all the protein structures containing bound Ca^{2+}, in addition to Mn^{2+} or Zn^{2+} (see "Experimental procedures"), and then analyzed for each metal ion to which residues it tends to bind and in what coordination number (Fig. 3, *a* and *b*; full data in Tables S1–S3). This analysis shows clear differences between the binding patterns of each metal: Zn^{2+} tends to be bound in a coordination number of 4, whereas both Mn^{2+} and Ca^{2+} are usually bound in a higher coordination number (5–6 and 6–7, respectively). In terms of preferred residues, Ca^{2+} shows very low preference to bind histidine residues, whereas Zn^{2+} shows high preference to histidine and cysteine, and Mn^{2+} is mostly bound to aspartate, followed by glutamate and histidine.

The canonical tetrahedral metal-binding site of the Zn^{2+}-transporting ZnT proteins is composed of a 2His–2Asp formation (4, 9). In contrast, the ZnT10 site is composed of Asn-Asp-His-Asp (Asn-43–Asp-47–His-244–Asp-248) (see Fig. 3, *c* and *d* and Fig. S1). As shown in Fig. 3*b*, Ca^{2+} has the highest preference to the Asn residue, followed by Mn^{2+}, whereas Zn^{2+} shows poor interaction with this residue. Thus, the ZnT10-binding site suggests more efficient transport of Mn^{2+} and Ca^{2+}, than of Zn^{2+}.

To determine whether Ca^{2+} drives Mn^{2+} transport by ZnT10 we applied the same functional criteria that we used to interrogate the H^+ or Na^+ transport. To monitor and distinguish between Mn^{2+} and Ca^{2+} fluxes we used Fura-2AM that can very effectively distinguish between Mn^{2+} and Ca^{2+} when excited at 360 nm or 340 nm/380 nm, respectively (28–30). To ascertain that we can distinguish between fluxes of these cations using a 360 nm *versus* 340 nm/380 nm spectral analysis, we monitored Mn^{2+} and Ca^{2+} influx (Fig. S3) induced by Ca^{2+} store depletion. Consistent with previous studies (28–30), Ca^{2+}, but not Mn^{2+}, influx was fluorescently monitored at a ratiometric 340 nm/380 nm excitation. Conversely Mn^{2+}, but not Ca^{2+}, influx was monitored when cells were excited at 360 nm (Fig. S3). Using this experimental paradigm, we then asked if extracellular Ca^{2+} can modulate the rate of Mn^{2+} transport by ZnT10 (Fig. 4, *a–c*). We found that Mn^{2+} influx was totally blocked when the cells were superfused with Mn^{2+} (5 μM) and Ca^{2+} (1.8 mM, initial phase of *purple trace*, Fig. 4, *a* and *c*) containing solution. Note that both Ca^{2+} and Mn^{2+} concentrations used are within the physiological range. In contrast, Mn^{2+} influx was observed in Ca^{2+}-free Ringer's solution (initial phase of *red trace*, Fig. 4, *b* and *c*). Accordingly, in cells loaded with Mn^{2+} (in the absence of Ca^{2+}), Mn^{2+} efflux depended on the presence of physiological Ca^{2+} (late phase of *red trace*, Fig. 4, *b* and *c*). Furthermore, Ca^{2+}-dependent Mn^{2+} efflux persisted even in the presence of extracellular Mn^{2+} (late phase of *brown trace*, Fig. 4, *b* and *c*). Thus, extracellular Ca^{2+} can effectively drive active cellular Mn^{2+} efflux, even against a steep inward Mn^{2+} gradient (Fig. 4*b*). If ZnT10 is mediating Ca^{2+}/Mn^{2+} exchange, it should manifest Ca^{2+} fluxes reciprocal to Mn^{2+} transport. We therefore monitored cytosolic Ca^{2+} by ratiometrically monitoring Fura-2AM at the Ca^{2+}-sensitive 340 nm/380 nm ratiometric excitation wavelength. We found that addition of Mn^{2+} to Ca^{2+}-free solution, led to a drop in cytosolic Ca^{2+} concentrations in ZnT10-expressing cells but not in vector transfected cells (Fig. 4, *d* and *e*). In the ZnT10-expressing cells, subsequent addition of Ca^{2+} led to robust Ca^{2+} influx (Fig. 4, *d* and *e*), thus manifesting a clear pattern of Mn^{2+}/Ca^{2+} exchange. Finally, we conducted a dose-response analysis of the extracellular Ca^{2+} concentrations required for driving Mn^{2+} efflux in cells loaded with Fura-2AM, excited at 360 nm, and found that the $K_{1/2}$ for Ca^{2+} is 0.97 ± 0.03 mM (Fig. 4, *f* and *g*). Thus our results indicate that the functional properties of ZnT10 are tailored for a physiological Ca^{2+}-driven Mn^{2+} exchange, promoting active cellular Mn^{2+} extrusion.

ZnT10 tetrahedral Asn-43 position determines a channel versus exchanger mode of transport

The canonical ZnT tetrahedral site contains a His residue, which is bigger than the Asn residue found in ZnT10 tetrahedral site (Asn-43, Fig. 3*d*), hence making the canonical ZnT site tighter for metal binding. This suggests that Asn-43 may be a key residue to control the mode of ion transport by ZnT10. We therefore compared the rates of transport by ZnT10 constructs mutated at the Asn-43 position. Note that all constructs were expressed, as determined by Western blot analysis (Fig. S2). We initially monitored Mn^{2+} influx (as described in Fig. 1*c*) in ZnT10 N43H, expressing cells, simulating the canonical site, and found that it does not mediate Mn^{2+} transport (N43H *blue trace*, Fig. 5, *a* and *b*). Similarly the ZnT10 N43D, mutant simulating the bacterial site (10), was nonfunctional (N43D *orange trace*, Fig. 5, *a* and *b*). In contrast, mutating the Asn-43 to a noncharged alanine (N43A *brown trace*, Fig. 5, *a* and *b*) or to a polar threonine (N43T *green trace*, Fig. 5, *b* and *c*) enhanced Mn^{2+} influx compared with WT ZnT10. We then asked if these mutations affect the coupling of Mn^{2+} to Ca^{2+} transport by monitoring Mn^{2+}-dependent Ca^{2+} efflux. We found that in cells expressing the ZnT10 N43A mutation, Mn^{2+}-dependent Ca^{2+} efflux was ~3-fold higher compared with WT ZnT10 (*brown trace*, Fig. 5, *d* and *f*), whereas the N43T mutation resulted in a significant decrease in Ca^{2+} efflux (*green trace*, Fig. 5, *d* and *f*). Our results therefore indicate that the Asn-43 position of ZnT10 controls the coupling of Mn^{2+} to Ca^{2+}. The N43A mutant enhances coupling between Mn^{2+} and Ca^{2+} exchange, whereas the N43T mutant induces uncoupled channel-like Mn^{2+} transport activity (Fig. 5, *c* and *d*). Consistent with this channel-like mode of the N43T mutant, comparison to WT ZnT10 kinetics showed that the apparent affinity of ZnT10 N43T to Mn^{2+} is lower and its maximal rate of Mn^{2+} transport is higher with respect to WT ZnT10 (Fig. 5, *e* and *f* and Table S5). Finally, we studied the role of the two additional residues on the tetrahedral site, ZnT10 His-244 and ZnT10 Asp-47. We found that even the conservative substitutions of ZnT10 H244D (mimicking other known bacterial Mn^{2+} CDF transporters; see Table S4) or ZnT10 D47E, were sufficient to eliminate Mn^{2+} transport (Fig. S3), indicating that similarly to other ZnTs these positions are essential and indispensable for metal cation selectivity and transport (4, 9, 31). Other mutations at these positions (ZnT10 D47A, ZnT10 H244A, ZnT10 D248A, ZnT10 D248A, and ZnT10 D248E) impaired ZnT10 expression and therefore are not included in the analysis (Fig. S3). Altogether, the results of this set of experiments identified ZnT10 Asn-43 position as a critical residue not only for promoting Mn^{2+} transport by ZnT10 but also for controlling an exchanger *versus* channel-like mode of ZnT10 transport (Fig. 5*g*).

Discussion

The results presented in this study show that ZnT10 is the first known transporter that harnesses the steep transmembrane Ca^{2+} gradient for active removal of Mn^{2+}, which is playing a double-edged sword role in cells. On the one hand, Mn^{2+} is an essential cofactor of many enzymes. On the other hand,

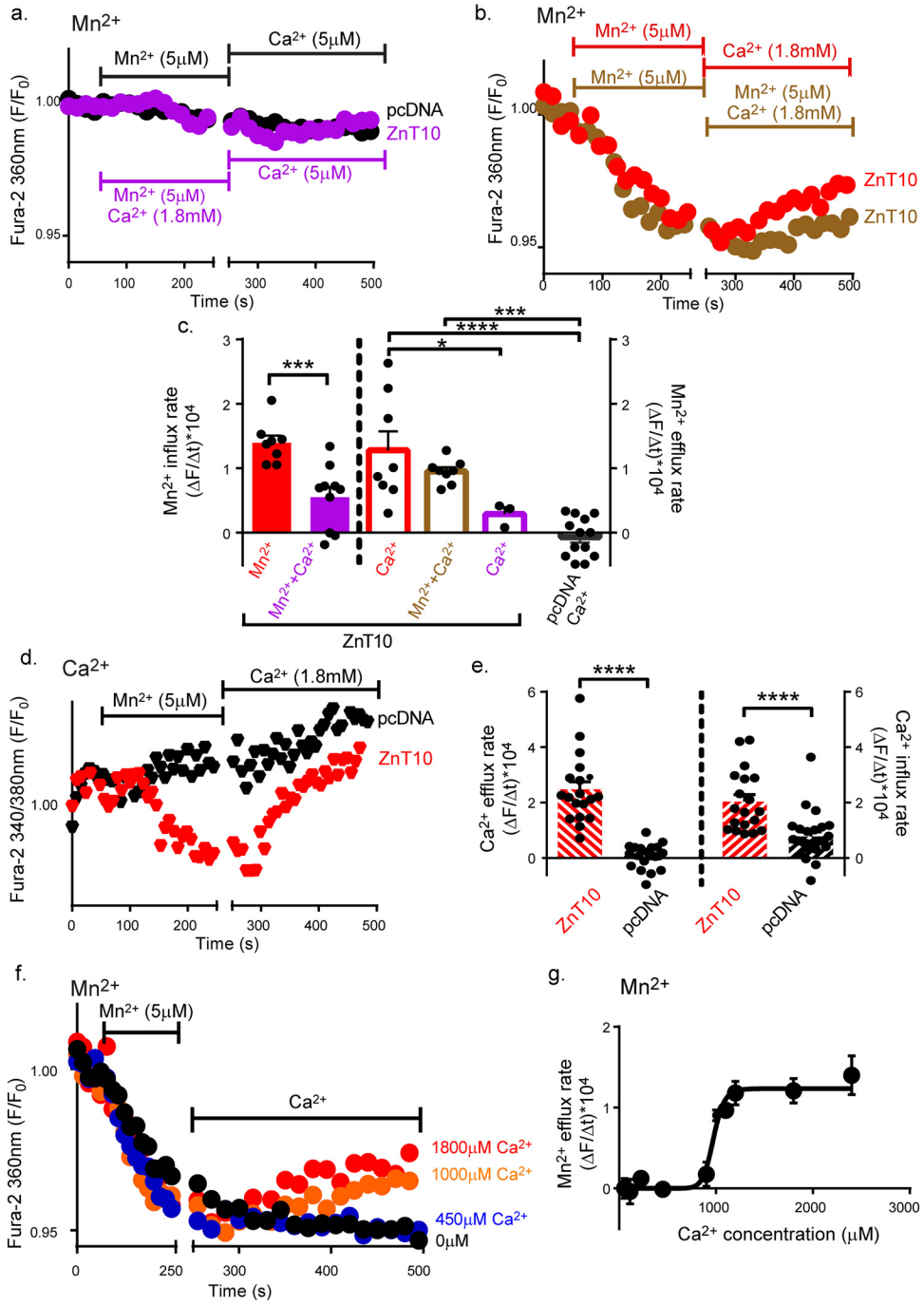

Figure 4. ZnT10 Mn^{2+} efflux is driven by Ca^{2+} influx. *a* and *b*, representative traces of Ca^{2+}-dependent Mn^{2+} exchange. Mn^{2+} transport was monitored in ZnT10 (*purple*, *red*, and *brown*) or pcDNA (*black*) transfected cells preloaded with Fura-2AM and excited at 360 nm as described in Fig. 1*c*. Cells were first superfused with Ringer's solution containing Mn^{2+} (5 μM) in the presence or absence of Ca^{2+} (1.8 mM) as indicated by the *left horizontal bar*, then superfused with Ringer's solution containing Ca^{2+} (1.8 mM) in the presence or absence of Mn^{2+} (5 μM) as indicated by the *right horizontal bar*. *c*, mean rates of cellular Mn^{2+} influx (unpaired *t*-test; *red*, $n = 8$; *purple*, $n = 10$) and efflux (one-way ANOVA test; *red*, $n = 8$; *brown*, $n = 8$; *purple*, $n = 3$; *black*, $n = 13$) values taken from *a* and *b* (****, $p < 0.0001$; ***, $p < 0.001$; *, $p < 0.05$). *d*, representative traces of Mn^{2+}-dependent Ca^{2+} transport. Changes in intracellular Ca^{2+} levels were monitored in ZnT10 (*red*) *versus* pcDNA (*black*) transfected cells. Cells were preloaded with Fura-2AM and excited at 340 nm and 380 nm (see "Experimental procedures"). Ringer's solution containing Mn^{2+} (5 μM) and Ca^{2+} (1.8 mM) were added as indicated by the *horizontal bars*. *e*, mean rates of cellular Ca^{2+} efflux and influx rates in ZnT10 (*red*, $n = 19$) *versus* pcDNA (*black*, $n = 25$) transfected cells taken from *d*. (unpaired *t*-test, ****, $p < 0.0001$). *f*, representative traces of Ca^{2+}-dependent Mn^{2+} fluxes dose-response analysis in ZnT10 transfected cells. Cells were loaded with Fura-2AM and excited at 360 nm as described in Fig. 1*c*. Cells were first superfused with Ca^{2+}-free Ringer's solution containing Mn^{2+} (5 μM) as shown by the *left horizontal bar* and then superfused with Ringer's solution containing the indicated Ca^{2+} concentrations. *g*, mean rates of cellular Ca^{2+}-dependent Mn^{2+} efflux taken from *f* at the indicated concentrations (allosteric sigmoidal fit; $n = 4$; $K_{1/2} = 973.6 \pm 29.98$, μM; $V_{max} = 1.234 \pm 0.08$, a.u.).

the presence of Mn^{2+} can be deleterious, triggering generation of harmful oxygen radicals, because of its physiological redox activity (32, 33). Therefore, cellular Mn^{2+} concentration must be tightly controlled. Mn^{2+} can enter cells via several cation channels and zip transporters (34, 35). Removal of Mn^{2+} is more challenging because it requires transport against its steep

gradient. Previous studies revealed that ZnT10 plays an important role in maintaining Mn^{2+} homeostasis. Mutations that diminish expression of ZnT10 have been linked to toxic accumulation of Mn^{2+} (14, 15). How ZnT10 can pump out Mn^{2+} against a major electrochemical gradient remained a major unanswered question. The hypothesis that Mn^{2+} extrusion is powered by Ca^{2+}-dependent exchange is supported by the following findings: 1) In the absence of extracellular Ca^{2+}, Mn^{2+} strongly permeates into ZnT10 expressing cells. 2) In the presence of both Ca^{2+} and Mn^{2+} in the extracellular solution, Mn^{2+} influx is blocked in ZnT10 expressing cells. 3) Addition of physiological Ca^{2+} concertation subsequent to Mn^{2+} influx reverses this process and triggers a Ca^{2+}-dependent Mn^{2+} efflux mediated by ZnT10. Thus ZnT10 manifests an exchange mechanism with a "classical" reverse and direct mode of operation. 4) Remarkably, Ca^{2+} can support Mn^{2+} influx by ZnT10 against an inward physiological gradient, thus supporting its role as a secondary active transporter, harnessing the Ca^{2+} gradient to power an active against-gradient extrusion of Mn^{2+}. 5) Transport of Mn^{2+} by ZnT10 is coupled to reciprocal Ca^{2+} transport. Thus, we find that influx of Mn^{2+} is linked to Ca^{2+} efflux, whereas ZnT10-dependent Mn^{2+} extrusion is linked to cellular Ca^{2+} influx. By all these criteria ZnT10 is acting as the first metal exchanger powered by extracellular Ca^{2+}. What is the physiological rational of switching ZnT10 mode of transport from H^+ coupled exchange (used by other ZnT members) to Ca^{2+}-dependent Mn^{2+} exchange? Although cytoplasmic level of Zn^{2+} is estimated in pM range, Mn^{2+} level may reach several orders of magnitude higher than Zn^{2+} (which is estimated in μM range). Moreover, although Zn^{2+} is relatively redox inert, Mn^{2+} has a physiologically relevant redox potential that may be highly toxic. Thus, the steep Ca^{2+} gradient compared with the modest H^+ gradient can support a more efficient exchange required to handle the higher Mn^{2+} concentrations. Our analysis (Fig. 3, *a–d*) further shows that the absence of His pairing at the metal transport site of ZnT10, replaced by Asn, supports a tighter Mn^{2+} than Zn^{2+} binding and may therefore facilitate the rate of Mn^{2+} transport compared with Zn^{2+} transport by other ZnT members (Table S3).

The versatility of the tetrahedral metal-binding site provides an excellent model for a comparative interrogation of structural-functional requirements of Mn^{2+} *versus* Zn^{2+} transport. We found that ZnT10 fully discriminates between Mn^{2+} and Zn^{2+} and does not conduct any apparent Zn^{2+} transport.

Our results show that pH has a strong regulatory effect on Mn^{2+} transport by ZnT10. The presence of a histidine residue in the transport site, which allows efficient binding only when unprotonated, might be one of the reasons for this. Such regulatory effect is shared by many other transporters and channels, for example NHE and Orai, and suggests a physiological role and pathophysiological implications. For example, cellular acidosis could be followed by impaired ZnT10 transport activity leading to toxic accumulation of Mn^{2+}. Intriguingly, previous studies linked brain acidosis to severity of neurodegenerative syndromes such as Alzheimer's disease (36–38) in which high Mn^{2+} concentrations are also found (39–41). Further studies are required to determine whether impaired Mn^{2+} homeostasis during neurodegeneration is linked to modulation of ZnT10 activity.

Finally, our results indicate that apart from conferring Mn^{2+} selectivity the ZnT10 Asn-43 position has an additional function. Substituting it with Thr (ZnT10 N43T) triggers rapid Mn^{2+} or Ca^{2+} fluxes that are independent of the presence of a counter trans ion. The specific change to Thr, compared with Ala and Asp, creates a similar-sized cavity and maintains the polarity of the site without adding extra charge, yet lowers the possible coordination number. This modification may preserve the capability to attract the cations but also allows a better, channel-like release of the ions. Thus, this position is required to couple Ca^{2+} and Mn^{2+} in the exchange mode mediated by ZnT10. Intriguingly, ZnT10 shares similar cation selectivity with Orai1. Both are highly selective for Mn^{2+} and Ca^{2+}, rejecting other metals, and the transport rates of both transporters are very modest compared with classical channels (35). A phylogenic analysis suggested that Orai1 shares a similar origin with CDF proteins (42); thus future physiological studies will determine whether they also share common transport sites or mode of operation.

Experimental procedures

Cell culture

HEK293-T cells were cultured in DMEM, supplemented with 10% FCS, 1% streptomycin and 1% penicillin. Cells were grown in either 25 cm^2 or 75 cm^2 flasks, in a humidified CO_2 incubator, at 37 °C. For live-cell imaging and immunocytochemistry experiments, cells were transferred onto glass coverslips, in 60-mm cell culture dishes. For immunoblotting, cells were transferred to 100-mm cell culture dishes.

Plasmid transfection

Plasmid transfection was performed as described previously (43). Amounts of plasmid (0.67 μg) used for transfection were calibrated by Western blotting.

Generation of mutants

The plasmids used in this study are variations of hZnT10 double-stranded plasmid. Site-directed mutagenesis was performed using the QuikChange Site-Directed Mutagenesis Kit (Stratagene) according to the manufacturer's protocol. All primers were designed using the primer design tool, on the University of Washington server, and manufactured by Sigma. The primers were as follows: ZnT10 N43H, CGACTCCTTCCACATGCTCTCCGACC; ZnT10 N43A, CCGACTCCTTCGCCATGCTCTCCGACC; ZnT10 N43T, CCGACTCCTTCACCATGCTCTCCGACC; ZnT10 N43D, CCGACTCTTCGACATGCTCTCCGACC; ZnT10 D47A, CAACATGCTCTCCGCCCTGATCTCGCTGTG; ZnT10 D47E, CATGCTCTCCGAGCTGATCTCGCTG; ZnT10 H244A, CAGAGGTGTACTTTTGGCTGTGATGGGAGATGC; ZnT10 H244D, CAGAGGTGTACTTTTGGATGTGATGGGAGATGCC; ZnT10 D248A, CTTTTGCATGTGATGGGAGCAGCCCTGGGGTCCGTGGTTG; ZnT10 D248E, CTTTTGCATGTGATGGGAGAAGCCCTG.

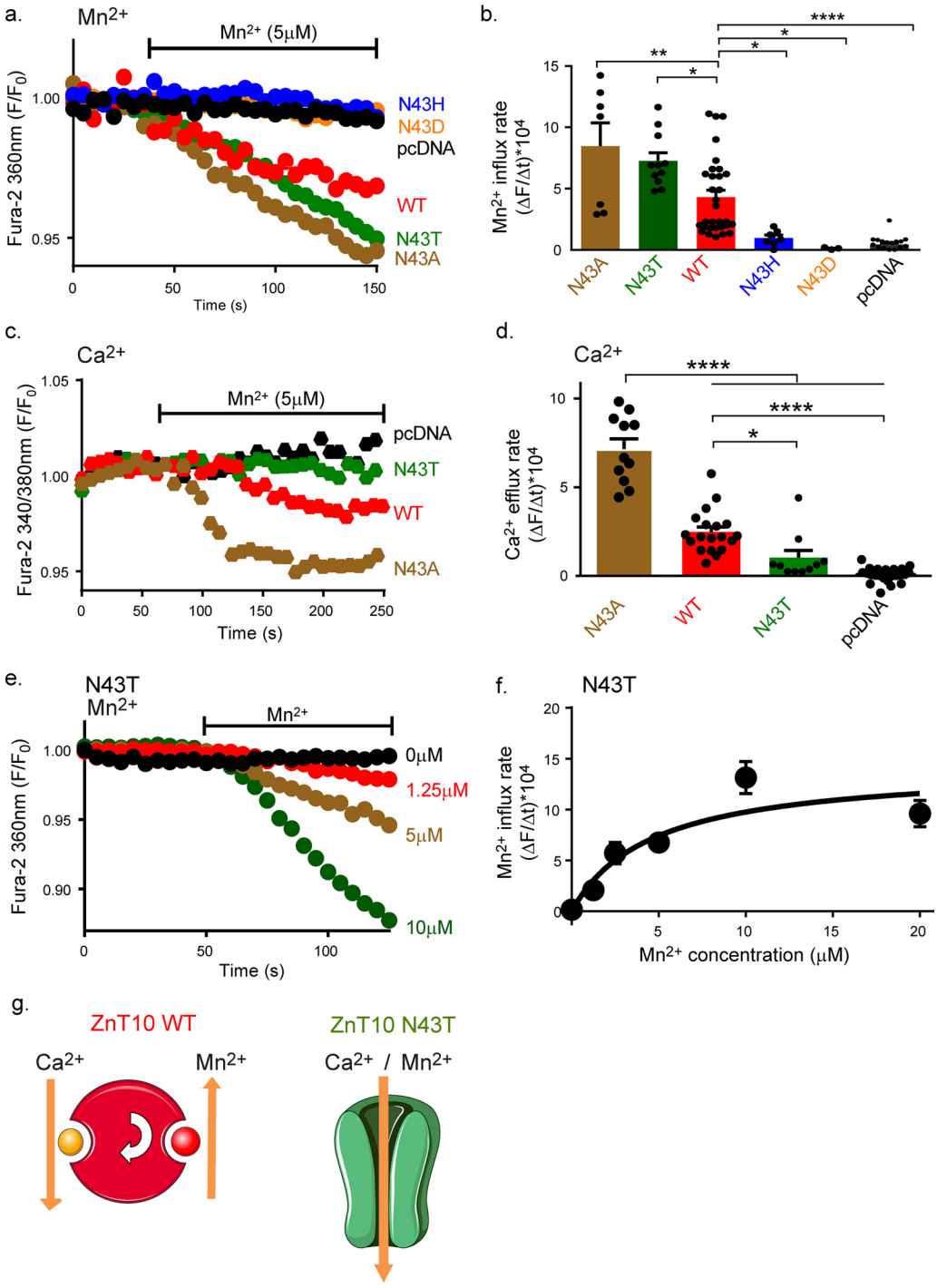

Figure 5. ZnT10 43 position controls exchange *versus* channel-like mode of operation by ZnT10. *a*, representative traces of Mn^{2+} influx in cell transfected with either ZnT10 WT (*red*), ZnT10 N43H (*blue*), ZnT10 N43D (*orange*), ZnT10 N43T (*green*), ZnT10 N43A (*brown*), or pcDNA (*black*) preloaded with Fura-2AM and excited at 360 nm. Cells were superfused with Ca^{2+}-free Ringer's solution and then Ringer's solution containing Mn^{2+} was added when indicated by the horizontal bar. *b*, mean rates of cellular Mn^{2+} influx for ZnT10 WT ($n = 31$), pcDNA ($n = 21$), ZnT10 N43H ($n = 7$), ZnT10 N43D ($n = 4$), ZnT10 N43T ($n = 11$), ZnT10 N43A ($n = 7$) taken from *a* (one-way ANOVA test; *, $p < 0.05$; **, $p < 0.01$; ****, $p < 0.0001$). *c*, representative traces of cytosolic Ca^{2+} efflux as described (Fig. 4*d*) in ZnT10 WT (*red*), pcDNA (*black*), ZnT10 N43T (*green*), and ZnT10 N43A (*brown*) transfected cells. *d*, mean rates of cellular Ca^{2+} efflux of ZnT10 WT (*red*, $n = 19$), pcDNA (*black*, $n = 25$), ZnT10 N43T (*green*, $n = 10$), or ZnT10 N43A (*brown*, $n = 11$) expressing cells taken from *c* (one-way ANOVA test; *$p < 0.05$; ****, $p < 0.0001$). *e*, dose-response analysis of Mn^{2+} transport by ZnT10 N43T mutant. Representative traces of Mn^{2+} influx in ZnT10 N43T transfected cells preloaded with Fura-2AM and exited at 360 nm. Cells were superfused with Mn^{2+} at the indicated concentration and Mn^{2+} influx was monitored as described in Fig. 1*e*. *f*, mean rates of cytoplasmic Mn^{2+} influx taken from *e* (Michaelis-Menten's fit; $n = 4$; $K_m = 4.61 \pm 1.815$, μM; $V_{max} = 14.25 \pm 2.294$, a.u.). *g*, schematic representation of ZnT10 and ZnT10 N43T acting as an exchanger and channel-like, respectively.

Immunoblot analysis

Cells were extracted using 200 μl of hot lysis buffer (1% SDS, 10 mM Tris-HCl, pH 8) per 100-mm plate and transferred to ice. A protease inhibitor mixture (Boehringer complete protease inhibitor mixture; Roche Applied Science) was added to the lysates, and protein concentrations were determined using the

modified Lowry procedure (44). SDS-PAGE and immunoblot analyses were performed, using the anti-ZnT10 (Abbexa) and anti-FLAG (GenScript) antibodies at dilutions of 1:2000. Secondary anti-mouse and anti-rabbit antibodies (Jackson ImmunoResearch Laboratories) were used at dilutions of 1:20000.

Fluorescence imaging

The imaging system consisted of an Axio Vert 100 inverted microscope (Zeiss), Polychrome 4 monochromator (TILL Photonics, Planegg, Germany), and a SensiCam cooled charge-coupled device (PCO, Kelheim, Germany).

Fluorescent imaging measurements were acquired with the Imaging Workbench 6 software (Axon Instruments, Foster City, CA) and analyzed using Microsoft Excel, KaleidaGraph, and GraphPad Prism 6. Cytoplasmic ion transport was determined in cells loaded with either 0.5 μM FluoZin-3 (Zn^{2+} assay), 2 μM Fura-2AM (Mn^{2+} and Ca^{2+} assays), or 1 μM BCECF-AM (H^+ assay). For Ca^{2+} assays, Mn^{2+} rates were monitored at excitation wavelengths of 360 nm as described previously (28). Ca^{2+} levels were monitored at 340 nm/380 nm (Fura-2AM). Note that while occupied by Ca^{2+}, Fura-2AM florescence will rise. In contrast, Mn^{2+} binding will reduce Fura-2AM florescence. Excited at the Ca^{2+} isosbestic point (360 nm), Fura-2AM is no longer sensitive to Ca^{2+} and reflects only Mn^{2+}-related changes. The 340 nm/380 nm fluorescence measurements would signal Ca^{2+} while canceling out most of the nonrelated Ca^{2+} signals (45).

Imaging experiments were conducted in the following way: Cells were superfused using Ringer's solution containing 130 mM NaCl, 20 mM Hepes, 15 mM glucose, 5 mM KCl, and 0.8 mM $MgCl_2$, with the pH adjusted to 7.4 (unless stated otherwise), supplemented with 1.8 mM $CaCl_2$ in Ca^{2+} Ringer's solution, 5 μM Mn^{2+} in Mn^{2+} Ringer's solution, or 50 μM Zn^{2+} in Zn^{2+} Ringer's solution.

For all single-cell imaging experiments, traces of averaged responses recorded from 5 to 25 cells in each experiment are shown. The rate of ion transport was calculated from each graph (summarizing an individual experiment) by a linear fit of the change in the fluorescence ($\Delta F/\Delta t$).

Sequence alignment

Sequences for data comparison were obtained using BLAST (46) and sequence alignments were constructed using the multiple sequence alignment program ClustalW (47).

Metals' amino acid preferences and coordination number analysis

Similarly to Barber-Zucker and others (31) a search for all known protein structures was conducted at the RCSB Protein Data Bank on May 2016. For each metal (Mn^{2+}, Zn^{2+}, and Ca^{2+}), the next parameters were used for PDB files filtration: Deposit structure had to contain protein, X-ray resolution was between 0 and 2.5 Å (so only X-ray structures with reliable resolution were used), and the PDB file had to contain a LINK entrance with the Atom label (Mn^2, Zn^{2+} or Ca^{2+}) in a metal coordination connection. For structures with more than 90% sequence identity, only a representative structure was retrieved.

In each structure, if there were symmetric binding sites, only one representative binding site for each metal was taken under consideration. If any ligand other than water (such as other metal ions, DNA molecules, or other small organic ligands) was bound to a metal cation, this metal was excluded from the statistic. Only metals that were bound by at least two atoms from a protein were considered.

Structural model of ZnT10

ZnT10 model was built using the SWISS-MODEL automatic modeling mode (13, 24, 25, 48), based on the structure of *Escherichia coli* YiiP (4) (PDB code: 3H90). Mutations have been implemented by Swiss-PdbViewer 4.1.0 (22) and the structural model figures were prepared using PyMOL (PyMOL Molecular Graphics System, Version 1.7.4, Schrödinger, LLC).

ZnT10 illustration

Illustration of ZnT10 was performed using the Servier Medical Art illustration resources.

Statistical analysis

All data were statistically analyzed by using GraphPad Prism 6 program. Statistical significance was determined by using the unpaired *t*-test with Welch's correction (confidence level = 95%) or one-way analysis of variance (ANOVA) test (Tukey's multiple comparisons test, confidence interval = 95%). Data dispersion were calculated as mean ± S.E.

Author contributions—M. L., N. E., and E. H. data curation; M. L., N. E., S. B.-Z., E. H., R. Z., and M. H. formal analysis; M. L. and N. E. investigation; M. L., R. Z., M. H., and I. S. writing-original draft; E. H. and I. S. conceptualization; E. H. methodology; R. Z., M. H., and I. S. writing-review and editing; M. H. and I. S. funding acquisition; I. S. supervision.

References

1. Huang, L., and Tepaamorndech, S. (2013) The SLC30 family of zinc transporters—A review of current understanding of their biological and pathophysiological roles. *Mol. Aspects Med.* **34,** 548–560 CrossRef Medline
2. Burch, R. E., Hahn, H. K., and Sullivan, J. F. (1975) Newer aspects of the roles of zinc, manganese, and copper in human nutrition. *Clin. Chem.* **21,** 501–520 Medline
3. Sekler, I., Sensi, S. L., Hershfinkel, M., and Silverman, W. F. (2007) Mechanism and regulation of cellular zinc transport. *Mol. Med.* **13,** 337–343 CrossRef Medline
4. Ohana, E., Hoch, E., Keasar, C., Kambe, T., Yifrach, O., Hershfinkel, M., and Sekler, I. (2009) Identification of the Zn^{2+} binding site and mode of operation of a mammalian Zn^{2+} transporter. *J. Biol. Chem.* **284,** 17677–17686 CrossRef Medline
5. Bosomworth, H. J., Adlard, P. A., Ford, D., and Valentine, R. A. (2013) Altered expression of ZnT10 in Alzheimer's disease brain. *PLoS One* **8,** e65475 CrossRef Medline
6. Lyubartseva, G., Smith, J. L., Markesbery, W. R., and Lovell, M. A. (2010) Alterations of zinc transporter proteins ZnT-1, ZnT-4 and ZnT-6 in preclinical Alzheimer's disease brain. *Brain Pathol.* **20,** 343–350 CrossRef Medline
7. Rutter, G. A., and Chimienti, F. (2015) SLC30A8 mutations in type 2 diabetes. *Diabetologia* **58,** 31–36 CrossRef Medline
8. Diabetes Genetics Initiative of Broad Institute of Harvard and MIT, Lund University, and Novartis Institutes of BioMedical Research, Saxena, R., Voight, B. F., Lyssenko, V., Burtt, N. P., de Bakker, P. I., Chen,

H., Roix, J. J., Kathiresan, S., Hirschhorn, J. N., Daly, M. J., Hughes, T. E., Groop, L., *et al.* (2007) Genome-wide association analysis identifies loci for type 2 diabetes and triglyceride levels. *Science* **316,** 1331–1336 CrossRef Medline

9. Hoch, E., Lin, W., Chai, J., Hershfinkel, M., Fu, D., and Sekler, I. (2012) Histidine pairing at the metal transport site of mammalian ZnT transporters controls Zn^{2+} over Cd^{2+} selectivity. *Proc. Natl. Acad. Sci. U.S.A.* **109,** 7202–7207 CrossRef Medline
10. Lu, M., and Fu, D. (2007) Structure of the zinc transporter YiiP. *Science* **317,** 1746–1748 CrossRef Medline
11. Nishito, Y., Tsuji, N., Fujishiro, H., Takeda, T. A., Yamazaki, T., Teranishi, F., Okazaki, F., Matsunaga, A., Tuschl, K., Rao, R., Kono, S., Miyajima, H., Narita, H., Himeno, S., and Kambe, T. (2016) Direct comparison of manganese detoxification/efflux proteins and molecular characterization of ZnT10 protein as a manganese transporter. *J. Biol. Chem.* **291,** 14773–14787 CrossRef Medline
12. Zogzas, C. E., Aschner, M., and Mukhopadhyay, S. (2016) Structural elements in the transmembrane and cytoplasmic domains of the metal transporter SLC30A10 are required for its manganese efflux activity. *J. Biol. Chem.* **291,** 15940–15957 CrossRef Medline
13. Chen, P., Bowman, A. B., Mukhopadhyay, S., and Aschner, M. (2015) SLC30A10: A novel manganese transporter. *Worm* **4,** e1042648 CrossRef Medline
14. Quadri, M., Federico, A., Zhao, T., Breedveld, G. J., Battisti, C., Delnooz, C., Severijnen, L. A., Di Toro Mammarella, L., Mignarri, A., Monti, L., Sanna, A., Lu, P., Punzo, F., Cossu, G., Willemsen, R., Rasi, F., Oostra, B. A., van de Warrenburg, B. P., and Bonifati, V. (2012) Mutations in SLC30A10 cause parkinsonism and dystonia with hypermanganesemia, polycythemia, and chronic liver disease. *Am. J. Hum. Genet.* **90,** 467–477 CrossRef Medline
15. Quadri, M., Kamate, M., Sharma, S., Olgiati, S., Graafland, J., Breedveld, G. J., Kori, I., Hattiholi, V., Jain, P., Aneja, S., Kumar, A., Gulati, P., Goel, M., Talukdar, B., and Bonifati, V. (2015) Manganese transport disorder: novel SLC30A10 mutations and early phenotypes. *Mov. Disord.* **30,** 996–1001 CrossRef Medline
16. Milne, D. B., Sims, R. L., and Ralston, N. V. (1990) Manganese content of the cellular components of blood. *Clin. Chem.* **36,** 450–452 Medline
17. Fernandes, J., Hao, L., Bijli, K. M., Chandler, J. D., Orr, M., Hu, X., Jones, D. P., and Go, Y. M. (2017) From the cover: Manganese stimulates mitochondrial H_2O_2 production in SH-SY5Y human neuroblastoma cells over physiologic as well as toxicologic range. *Toxicol. Sci.* **155,** 213–223 CrossRef Medline
18. Smith, M. R., Fernandes, J., Go, Y. M., and Jones, D. P. (2017) Redox dynamics of manganese as a mitochondrial life-death switch. *Biochem. Biophys. Res. Commun.* **482,** 388–398 CrossRef Medline
19. Mindell, J. A. (2012) Lysosomal acidification mechanisms. *Annu. Rev. Physiol.* **74,** 69–86 CrossRef Medline
20. Boron, W. F., and Boulpaep, E. L. (2005) *Medical Physiology: A Cellular and Molecular Approach*, updated 2nd ed., Elsevier Saunders, Philadelphia, PA.
21. Simons, T. J. (1988) Calcium and neuronal function. *Neurosurg. Rev.* **11,** 119–129 CrossRef Medline
22. Bosomworth, H. J., Thornton, J. K., Coneyworth, L. J., Ford, D., and Valentine, R. A. (2012) Efflux function, tissue-specific expression and intracellular trafficking of the Zn transporter ZnT10 indicate roles in adult Zn homeostasis. *Metallomics* **4,** 771–779 CrossRef Medline
23. Patrushev, N., Seidel-Rogol, B., and Salazar, G. (2012) Angiotensin II requires zinc and down-regulation of the zinc transporters ZnT3 and ZnT10 to induce senescence of vascular smooth muscle cells. *PLoS One* **7,** e33211 CrossRef Medline
24. Kambe, T., Narita, H., Yamaguchi-Iwai, Y., Hirose, J., Amano, T., Sugiura, N., Sasaki, R., Mori, K., Iwanaga, T., and Nagao, M. (2002) Cloning and characterization of a novel mammalian zinc transporter, zinc transporter 5, abundantly expressed in pancreatic β cells. *J. Biol. Chem.* **277,** 19049–19055 CrossRef Medline
25. Leyva-Illades, D., Chen, P., Zogzas, C. E., Hutchens, S., Mercado, J. M., Swaim, C. D., Morrisett, R. A., Bowman, A. B., Aschner, M., and Mukhopadhyay, S. (2014) SLC30A10 is a cell surface-localized manganese efflux transporter, and parkinsonism-causing mutations block its intracellular trafficking and efflux activity. *J. Neurosci.* **34,** 14079–14095 CrossRef Medline
26. Roth, J. A. (2006) Homeostatic and toxic mechanisms regulating manganese uptake, retention, and elimination. *Biol. Res.* **39,** 45–57 Medline
27. Ohana, E., Segal, D., Palty, R., Ton-That, D., Moran, A., Sensi, S. L., Weiss, J. H., Hershfinkel, M., and Sekler, I. (2004) A sodium zinc exchange mechanism is mediating extrusion of zinc in mammalian cells. *J. Biol. Chem.* **279,** 4278–4284 CrossRef Medline
28. Kwakye, G. F., Li, D., Kabobel, O. A., and Bowman, A. B. (2011) Cellular fura-2 manganese extraction assay (CFMEA). *Curr. Protoc. Toxicol.* **48,** 12.18.1–12.18.20 CrossRef Medline
29. Ward, M. L., Pope, A. J., Loiselle, D. S., and Cannell, M. B. (2003) Reduced contraction strength with increased intracellular $[Ca^{2+}]$ in left ventricular trabeculae from failing rat hearts. *J. Physiol.* **546,** 537–550 CrossRef Medline
30. Fonteríz, R. I., López, M. G., García-Sancho, J., and García, A. G. (1991) Alamethicin channel permeation by Ca^{2+}, Mn^{2+} and Ni^{2+} in bovine chromaffin cells. *FEBS Lett.* **283,** 89–92 CrossRef Medline
31. Barber-Zucker, S., Shaanan, B., and Zarivach, R. (2017) Transition metal binding selectivity in proteins and its correlation with the phylogenomic classification of the cation diffusion facilitator protein family. *Sci. Rep.* **7,** 16381 CrossRef Medline
32. Martinez-Finley, E. J., Gavin, C. E., Aschner, M., and Gunter, T. E. (2013) Manganese neurotoxicity and the role of reactive oxygen species. *Free Radic. Biol. Med.* **62,** 65–75 CrossRef Medline
33. Farina, M., Avila, D. S., da Rocha, J. B. T., and Aschner, M. (2013) Metals, oxidative stress and neurodegeneration: A focus on iron, manganese and mercury. *Neurochem. Int.* **62,** 575–594 CrossRef Medline
34. Aydemir, T. B., Kim, M. H., Kim, J., Colon-Perez, L. M., Banan, G., Mareci, T. H., Febo, M., and Cousins, R. J. (2017) Metal transporter Zip14 (Slc39a14) deletion in mice increases manganese deposition and produces neurotoxic signatures and diminished motor activity. *J. Neurosci.* **37,** 5996–6006 CrossRef Medline
35. Bird, G. S., DeHaven, W. I., Smyth, J. T., and Putney, J. W., Jr. (2008) Methods for studying store-operated calcium entry. *Methods* **46,** 204–212 CrossRef Medline
36. Basurto-Islas, G., Grundke-Iqbal, I., Tung, Y. C., Liu, F., and Iqbal, K. (2013) Activation of asparaginyl endopeptidase leads to Tau hyperphosphorylation in Alzheimer disease. *J. Biol. Chem.* **288,** 17495–17507 CrossRef Medline
37. Pirchl, M., and Humpel, C. (2009) Does acidosis in brain play a role in Alzheimer's disease? [In German]. *Neuropsychiatr.* **23,** 187–192 Medline
38. Ruffin, V. A., Salameh, A. I., Boron, W. F., and Parker, M. D. (2014) Intracellular pH regulation by acid-base transporters in mammalian neurons. *Front. Physiol.* **5,** 43 CrossRef Medline
39. Hare, D. J., Faux, N. G., Roberts, B. R., Volitakis, I., Martins, R. N., and Bush, A. I. (2016) Lead and manganese levels in serum and erythrocytes in Alzheimer's disease and mild cognitive impairment: Results from the Australian Imaging, Biomarkers and Lifestyle Flagship Study of Ageing. *Metallomics* **8,** 628–632 CrossRef Medline
40. Markesbery, W. R., Ehmann, W. D., Hossain, T. I., and Alauddin, M. (1984) Brain manganese concentrations in human aging and Alzheimer's disease. *Neurotoxicology* **5,** 49–57 Medline
41. Tong, Y., Yang, H., Tian, X., Wang, H., Zhou, T., Zhang, S., Yu, J., Zhang, T., Fan, D., Guo, X., Tabira, T., Kong, F., Chen, Z., Xiao, W., and Chui, D. (2014) High manganese, a risk for Alzheimer's disease: High manganese induces amyloid-β related cognitive impairment. *J. Alzheimers Dis.* **42,** 865–878 CrossRef Medline
42. Matias, M. G., Gomolplitinant, K. M., Tamang, D. G., and Saier, M. H., Jr. (2010) Animal Ca^{2+} release-activated Ca^{2+} (CRAC) channels appear to be homologous to and derived from the ubiquitous cation diffusion facilitators. *BMC Res. Notes* **3,** 158 CrossRef Medline
43. Palty, R., Silverman, W. F., Hershfinkel, M., Caporale, T., Sensi, S. L., Parnis, J., Nolte, C., Fishman, D., Shoshan-Barmatz, V., Herrmann, S., Khananshvili, D., and Sekler, I. (2010) NCLX is an essential component of

mitochondrial Na^+/Ca^{2+} exchange. *Proc. Natl. Acad. Sci. U.S.A.* **107,** 436–441 CrossRef Medline

44. Markwell, M. A., Haas, S. M., Bieber, L. L., and Tolbert, N. E. (1978) A modification of the Lowry procedure to simplify protein determination in membrane and lipoprotein samples. *Anal. Biochem.* **87,** 206–210 CrossRef Medline
45. Grynkiewicz, G., Poenie, M., and Tsien, R. Y. (1985) A new generation of Ca^{2+} indicators with greatly improved fluorescence properties. *J. Biol. Chem.* **260,** 3440–3450 Medline
46. Altschul, S. F., Gish, W., Miller, W., Myers, E. W., and Lipman, D. J. (1990) Basic local alignment search tool. *J. Mol. Biol.* **215,** 403–410 CrossRef Medline
47. Thompson, J. D., Higgins, D. G., and Gibson, T. J. (1994) CLUSTAL W: Improving the sensitivity of progressive multiple sequence alignment through sequence weighting, position-specific gap penalties and weight matrix choice. *Nucleic Acids Res.* **22,** 4673–4680 CrossRef Medline
48. Lu, M., Chai, J., and Fu, D. (2009) Structural basis for autoregulation of the zinc transporter YiiP. *Nat. Struct. Mol. Biol.* **16,** 1063–1067 CrossRef Medline